Journal of Scientific Research & Reports

26(10): 93-106, 2020; Article no.JSRR.63908
ISSN: 2320-0227

Theoretical Analysis of the Bladeless Wind Turbine Performance

A. Anthony Adeyanju[1*] and D. Boucher[1]

[1]Mechanical Engineering Department, University of West Indies, St. Augustine, Trinidad and Tobago.

Authors' contributions

This work was carried out in collaboration between both authors. Authors AAA and DB worked on every aspect of the manuscript. Both authors read and approved the final manuscript.

Article Information

DOI: 10.9734/JSRR/2020/v26i1030325
Editor(s):
(1) Dr. Rahul Kumar Jaiswal, National Institute of Hydrology, India.
Reviewers:
(1) Venkata Sanyasi Seshendra Kumar Karri, GITAM University, India.
(2) Kadhim Fadhil Nasir, Al-Furat Al-Awsat Technical University, Iraq.
Complete Peer review History: http://www.sdiarticle4.com/review-history/63908

Original Research Article

Received 25 October 2020
Accepted 30 December 2020
Published 31 December 2020

ABSTRACT

A bladeless wind turbine utilizes vortex formation to extract energy from the wind. Vortex formation are small swirls of air which occur as a result of the geometric shape of the device. This study designed a bladeless wind turbine which incorporates a structural support at a distance offset from the center axis of the cylindrical mast. Springs were added to the final design as means to provide the stiffness required to obtain resonance with the vortex shedding frequency and to also assist in supporting the structure. The analysis was conducted at wind speeds 1m/s, 4m/s and 7m/s, where the geometrical properties of the device remained constant. MATLAB was used to analyze the equation of motion derived for the device. The variables of interest in the studies were mainly the angular acceleration, power coefficient and the resonant frequency. The results obtained showed that for wind speeds above and below the designed wind speed of 4m/s the angular velocity remained the same. Results of this model showed that high amplitudes occur only at resonance. Results showed that with the current power generating mechanism, the average efficiency attainable is approximately 2% at steady state. This is the theoretical efficiency which could be achieved based on the current model. It was discovered that for linearly tapered cylinders, increased oscillations occurred during the 'lock-in range' for a range of reduced velocities. The reduced velocity of the designed wind speed is approximately Vr = 5m/s. This value lies within the theoretical range lock in range where increased oscillations are expected to occur between reduced velocities of 4.75m/s and 8m/s [1].

**Corresponding author: E-mail: Anthony.adeyanju@sta.uwi.edu;*

Keywords: Wind turbine; vortex; vibration analysis model; energy.

1. INTRODUCTION

The world is suffering severely from an energy crisis due to climate change, global warming and depleting oil reserves. According to British Petroleum, at current extraction rates, the world's oil reserves are estimated to last until 2072. Renewable energy devices now play a critical role in the development of countries around the world. Governments are investing heavily in the renewable energy sector to meet the current global energy demands with expectancy to reduce use of natural gas, coal and so forth [2].

Caribbean countries in recent years have been focusing heavily on renewable energy projects such as large solar and wind energy farms to generate electricity to be added to the grid. These are ongoing initiatives require high capital which can potentially increase the cost of electricity on a domestic level.

Traditional wind turbines present numerous challenges such as high capital cost, maintenance cost, transportation cost and noise has proven to be an issue for civilians. Through continuous research and development, innovative designs have been discovered to alleviate such issues. One proposed device is the Bladeless Wind Turbine whose energy is harnessed from Vortex Induced Vibrations. This wind turbine has no blades and less moving parts hence it is quieter, easier to build and cheaper to manufacture.

Bladeless Wind Turbines is a recent technology where research is still being conducted to analyze the performance capabilities of such a device for large scale energy production. At this current stage, the turbine is most suitable for off grid applications which don not require high electrical demand.

Bladeless wind turbines operate due to periodic forces produced by the vortex shedding phenomenon. These vortices occur as the wind hits the structure of the turbine shedding at a wind dependent frequency. The unpredictability of fluctuating wind speeds can affect its performance due to the following:

1. If the oscillations of the turbine are not amplified or harnessed correctly to work cohesively with a power generating unit, the device will not be able to produce a steady voltage output.
2. The vortex shedding frequency changes, hence, we obtain maximum amplitude of the turbine when resonance occur. When the vortex shedding frequency increases below or above the natural frequency of the structure, we have less oscillations and hence losses within the system.

As a result, by amplifying the oscillations of the turbine which is directly due to the synchronized frequency between the wind and the structure indicates that adjusting the natural frequency of the system during operation will enhance its performance where the electrical generating unit will provide a reliable voltage output.

Therefore, investigating and developing improvements to current designs to increase the efficiency and reliability of this device for use in rural areas can aid in renewable energy applications for the Caribbean. For example, farming, to power greenhouse sensors, night lighting and so forth.

2. REVIEW OF LITERATURE

2.1 Vortex Shedding Phenomenon

Naturally, for any bluff body (a structure as a result of its shape has a separated flow over its surface; *cylinder*) placed in a uniform flow with changing velocity, will develop a thin boundary layer along its body surface due to the viscosity of the fluid. This boundary layer develops until it reaches a critical point termed the separation point, where the fluid particles overlap resulting in a wake region behind the body as shown in Fig. 1. This wake region is commonly termed as the 'Kármán Vortex Street' where periodic shedding of these vortices from the surface of the body induces periodic pressure differentials on the structure [3].

The relationship between the vortex shedding frequency, diameter of the cylinder and the velocity of the ambient flow has been discovered by Strohaul almost exactly 100 years ago in connection with his work in a special method of creation of sound [1]. The strohaul number is a dimensionless quantity as like the Reynold's number which is the ratio of the inertial forces to viscous forces of a fluid. It was Lord Rayleigh, a

British scientist who discovered that the Strohaul number is a function of the Reynold's number for a given body and it should be defined as,

$$S_t(Re) = \frac{f_w D}{V} \quad (1)$$

S_t- Strohaul number
R_e- Reynold's number
f_w– Frequency of vortex shedding
D- Diameter of cylinder
V- Velocity of ambient fluid

2.2 Analysis of Vortex Induced Vibrations (VIV)

Cross flow induced vibrations have plagued engineers for years and it has proven to be one of the most important problems in various fields. Flow induced vibrations describes the interaction that occurs between a fluid's dynamic forces and a structure's inertial, damping and elastic forces [4]. Researchers often if not most of the time try to either avoid or suppress the large amplitudes which occur in VIV but for the case of vibration energy harvesting the goal is to achieve such conditions.

For a cylinder subjected to a cross flow, vibration is expected in two directions, transverse and parallel to the flow. Vibrations transverse to the flow is defined as lift while the former is defined as drag. Each direction has its associated frequency where in the transverse direction for a given velocity this frequency is more dominant. The frequency in the transverse direction is the vortex shedding frequency and it can be obtained by use of equation (1). In the drag direction the frequency is twice the vortex shedding frequency [4].

It has been proven that when the vortex shedding frequency (f_w) approaches the natural frequency (f_n) of an elastic rigid cylinder, resonance occurs where we have increased oscillation of the body for a range of velocities. This phenomenon is termed as the 'synchronization range'. Semi-empirical and of recent, CFD methods, have been used extensively to create models that can be used to help understand and predict the occurrence of this phenomenon. The oscillation of the turbine can be modelled as a *single degree of freedom system (1DOF)* where equation (2) describes the motion of the cylinder in the Y (transverse) direction [5].

$$m\ddot{y} + 2\zeta\omega_n\dot{y} + {\omega_n}^2 y = {C_L\rho U^2 D}/{2} \quad (2)$$

For a circular cylinder undergoing oscillating flow, the magnitude and occurrence of oscillations and range of synchronization for a given body depend heavily on the *lift coefficient (C_L), reduced velocity (V_r) and reduced damping (C_n).*

$$V_r = \frac{V}{f_n D} \quad (3)$$

$$C_n = \frac{4\pi m\zeta}{\rho D^2} \quad (4)$$

$$C_L = \frac{F}{{1}/{2}\rho U^2 D} \quad (5)$$

Where,
f_n - natural frequency of cylinder
D- diameter of cylinder
M- cylinder mass
ζ – damping ratio
F- force induced by surrounding fluid
ρ- air fluid density

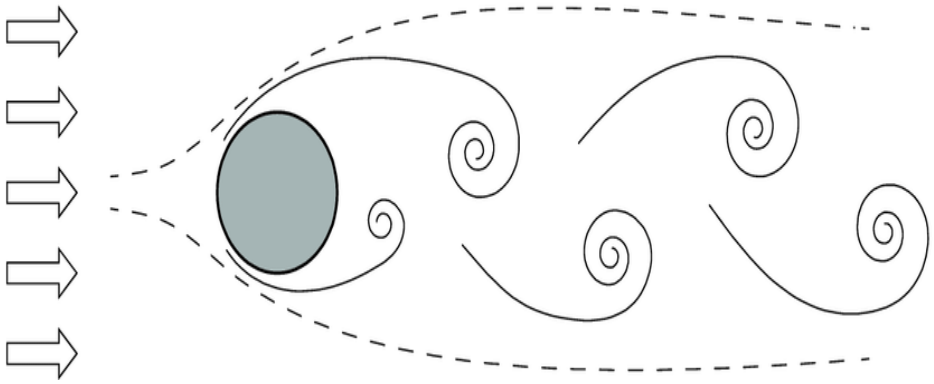

Fig. 1. Vortex Street Generation [3]

For cross flow oscillations in air, the excitation range extends over 4.75 <V_r < 8 where maximum amplitudes occur in the range 5.5 < V_r < 6.5 [1]. In addition, two regimes of Re desirable for vortex shedding are values of 40 ≤ Re ≤ 90 and 90 ≤ Re ≤ 150 [6]. At such low subcritical Reynolds numbers, we have laminar vortex shedding where the strouhaul number is approximately 0.2 for smooth cylinders. Vortex formation is also evident under turbulent flow. The regime under which this occurs is 300 < Re < 3x 10^5 [6].

Fig. 2 shows the image of Reynolds number regimes for vortex shedding while the relationship between Strohaul number and Reynolds umber is shown in Fig. 3. The Strohaul number was used in current studies where only small variations occur for large Reynold's numbers.

2.3 Factors Affecting Performance

2.3.1 Efficiency

For conventional horizontal axis wind turbine (HAWT), Betz's Limit states that the maximum efficiency which can be attained for a turbine is 59%. Betz's limit is seen as a benchmark for wind energy conversion systems. For VIV wind turbines the efficiency is defined as the ratio of the mean power imparted by the flow to the body per unit length, $P_{F\text{-}B}$ equation (6) and the total power in the flow per unit length P_F, equation (7) [7]. The power captured in the tower of the turbine is greater than the electrical power output from the generating unit due to losses of the system. This must also be taken into consideration when calculating the turbine performance [8].

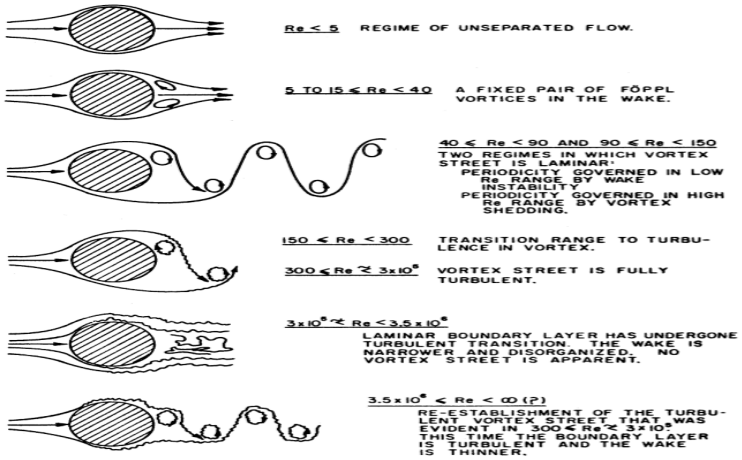

Fig. 2. Image of Reynold's number regimes for vortex shedding [6]

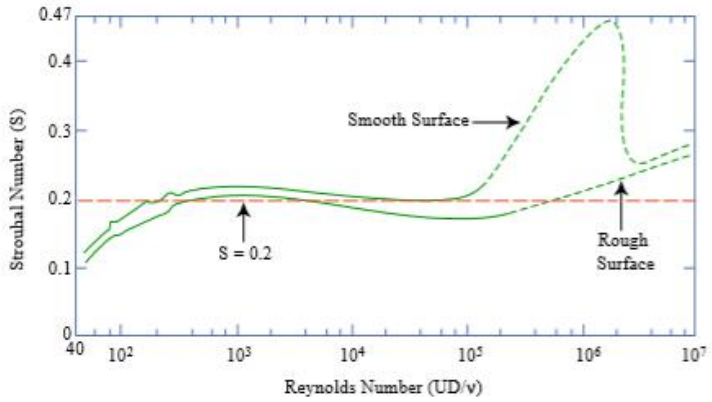

Fig. 3. Relationship between Strohaul number and Reynold's number [5]

$$P_{F-B} = {}^{1}/_{2}\,\rho U^{3} D \quad (6)$$

$$P_{F-B} = {}^{1}/_{T}\int_{0}^{T} F_{y}\dot{y}\,dt \quad (7)$$

$$\eta = \frac{P_{F-B}}{P_{F}} \quad (8)$$

2.3.2 Aerodynamics

Aerodynamic forces are a fundamental factor as it pertains to the design of aero-mechanical structures. The two major aerodynamic forces acting on a body undergoing VIV are lift and drag forces [9]. At low wind speeds, lift forces are desirable since the power produced by the turbine is a result of lift force. A high lift to drag ratio is best suited for the design of the turbine mast. C_L- Lift coefficient, C_D- Drag coefficient [8].

$$Lift\ to\ Drag\ Ratio = \frac{C_L}{C_D} \quad (9)$$

2.3.3 Taper ratio

As it pertains to oscillations of a cylinder in a cross flow, there is a significant difference in vortex formation based on the type of cylinder. There are two main type of cylinders used for analysis, uniformed cylinders of a constant diameter and tapered cylinders which have a minimum and maximum diameter. The amplitude response of oscillations differs in both geometries and this is a result of two modes of vortex shedding [10]. Research has shown that the uniform cylinder experiences a mode of vortex formation referred to as 2S vortex shedding while the tapered cylinder experiences hybrid shedding which is a combination of 2S and 2P shedding. 2S shedding refers to two single vortices or swirls of air being formed per second and 2P refers to two pairs of vortices being shed per second. Each formation affects the oscillation of the turbine differently. Research conducted by [10] showed that the tapered cylinder provides higher amplitudes when compared to the uniform cylinder. In addition, it was shown for the tapered cylinders, as the taper ratio is decreased the lock in range started at higher recued velocities (Vr) and this range extended through higher reduced velocities. Fig. 4 shows the amplitude and frequency ratio response for three taper ratios or 29,10, 17 and ∞ represents the uniform cylinder.

2.3.4 Tuning system

The general requirement of the VIV turbine is that the device operates in resonance at the excitation frequency of the wind. This limits the maximum performance of the turbine to a short range of frequencies (synchronization range). Basic mechanical vibration theory indicates that to adjust the natural frequency of a system, either; (i) adjust the mass or (ii) adjust the stiffness of the system. The first option is deemed infeasible to achieve while the device is in operation.

A proposed tuning system technique uses four permanent magnets oriented such that two of the magnets repel each other while the remaining two attract each other. The applied magnetics force alters the effective stiffness of the structure. *This magnetic force is dependent on the distance between the magnets* [11]. The additional stiffness induced from the magnetic force is positive for repulsive force and negative for attractive force (Fig. 5). On the flip side, one must consider the energy requirements of active tuning and the corresponding implications on the overall efficiency of the system [11].

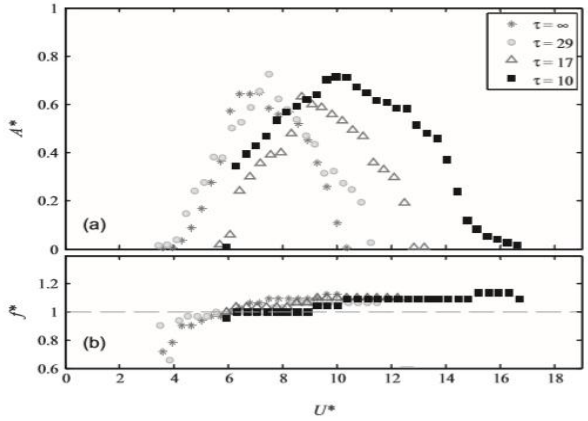

Fig. 4. Response of tapered vs uniform cylinders [10]

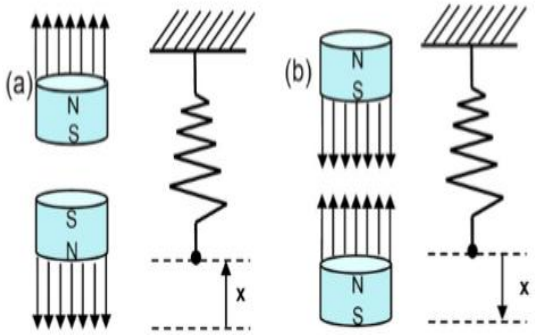

Fig. 5. Image of spring equivalent; (a) repulsive (+ve), (b) attractive(-ve) [11]

3. METHODOLOGY

An exploded view of the linkage mechanism of the bladeless wind turbine is shown in Fig. 6. It consists of the following:

Two (2) extension springs
Modification of the joint mechanism
Force joint disc
Connecting rod
Connecting Disc.

In order to convert the random oscillatory motion of the cylindrical mast to consistent linear motion of the permanent magnet, each part of this mechanism plays an important role. The mechanism is designed in such a way to ensure the oscillation of the cylinder is kept regardless of the direction of the wind. The mechanism will lie closely under the cylinder to maximize on the energy transfer from the wind to the system. The socket joint (4) could be fixed to any rigid surface to ensure stability of the ball joint at (3). This is the main anchor of the entire system. The extension springs (6) can be hooked to any adjacent surface and then hooked to the connecting rod of the joint at (10). These springs serve to provide the required stiffness to the system to assist with its stability and by extension its natural frequency.

The connecting rod at (1) is fitted onto the connecting disc (2) and then screwed to the joint at (3). The connecting disc is fitted to the base of the cylinder and this serves as a fixed point to secure the cylinder in position. The ball joint (7) is fitted into the socket at (8) and the force disc (5) is clipped around the top of the joint to lock the joint. The permanent magnet at (9) is screwed into the base of the socket joint (8) with a countersunk screw. As the linkage system oscillates the magnet will move in a linear direction with the assistance of the collar blocks (6). The blocks are fixed together with two spokes (4) as shown in Fig. 7. As the magnet oscillates in the groove of the block, the magnetic flux will cut the two conductive windings (5) to induce an EMF.

3.1 Operation of Bladeless Wind Turbine

The cylindrical mast will oscillate freely about the ball joint mechanism as the vortices are formed. As the cylinder oscillates, this energy is transferred to the rod of the joint at (3) which results in the translation and rotation of the ball and socket joint immediately below. The force disc at (5) is essential to ensure that this transfer of energy occurs from the mast to the joint. The joint (7) will oscillate in the same sense of direction as the cylinder but when this occurs, a force will be exerted on the force disc as seen by the intersection of the CAD models shown in Fig. 8 at point (A). Therefore, in simple terms, the joint has the degrees of freedom of a ball joint, but it will behave like a hinged/pin joint. The arrows in blue indicates the direction of motion of each joint. This is how the motion of the permanent magnet will be obtained.

4. THEORETICAL ANALYSIS OF THE BLADELESS WIND TURBINE PERFORMANCE

Equation (10) represents the equation of motion of the cylinder for angular oscillations about the pivot point ‘O’. By solving this equation, the angular displacement and velocity can be obtained. These values can be used to predict the speed of the attached magnets which can then be used to estimate the theoretical efficiency and power generated under various loads.

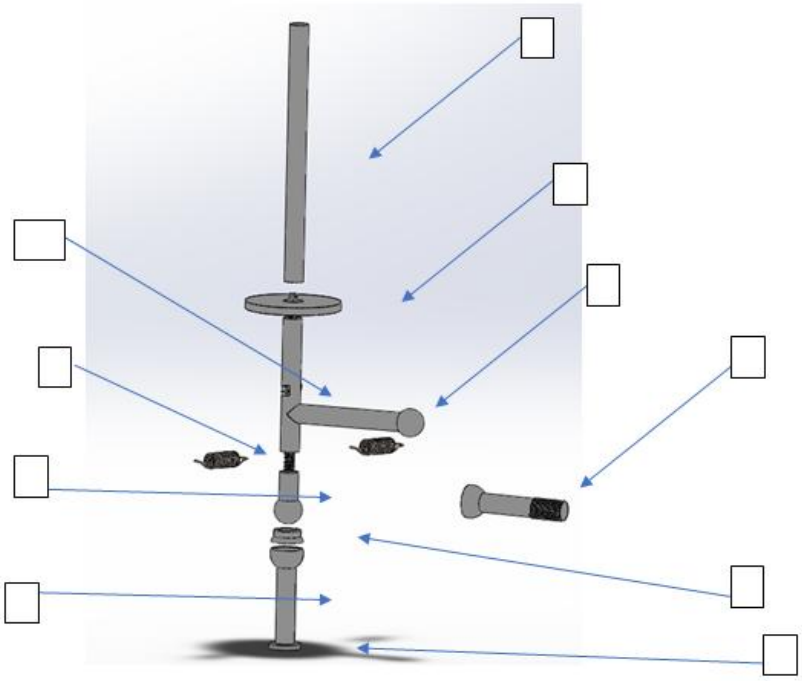

Fig. 6. Exploded view of bladeless wind turbine mechanism

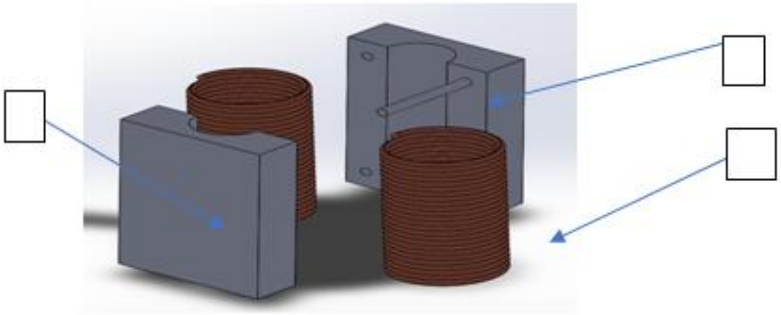

Fig. 7. Slider block and coils

4.1 Solution of Equation of Motion

For any un-damped system, the solution to the equation of motion comprises of the two parts, the steady state solution and the transient solution. For the sake of accuracy, both parts were used to obtain the general solution where,

$$\theta = \theta_t + \theta_s \quad (10)$$

$$\theta = A\cos(\omega_n t) + Bsin(w_n t) + \frac{M_o}{k(1-r^2)}\sin(\omega_s t) \quad (11)$$

$$r = \frac{\omega_s}{\omega_n} \quad (12)$$

Take the first and second derivative of equation (12) to obtain the angular velocity and acceleration.

$$\dot{\theta} = \omega_n A\, sin(w_n t) - w_n Bcos(w_n t) - \omega sMok1{-}r2coswst \quad (13)$$

$$\ddot{\theta} = A\,{\omega_n}^2\cos(\omega_n t) + B{\omega_n}^2 sin(w_n t) + \omega s2Mok1{-}r2\sin(\omega st) \quad (14)$$

$$let\ C = \frac{\omega_s M_o}{k(1-r^2)} \quad (15)$$

Equations (13) and (14) will be used for further analysis of the system. First the coefficients A and B must be determined by using the initial conditions. We let $\theta_t = 0$, take the first and second derivative then substitute the initial conditions.

At t=0
$\theta_{t=0} = 0.5\ rad$
$\ddot{\theta}_{t=0} = 1.5\ {}^{rad}/_{s}$

This results in the coefficients equating to A= 0.5 and B = 0.035791. The coefficients B and C are dependent on the frequency ratio and the natural frequency of the system respectively.

4.2 Determination of the Magnet Speed

The velocity of the magnet is required to calculate the change in magnetic flux. This change in magnetic flux will induce an EMF into the conduction coils as shown in Fig. 9. To determine the speed of the magnet an equation of motion for the distance travelled must be developed. The first derivate of this equation is taken to obtain an equation for velocity.
Assumptions:

The system is a rigid body.

The angular displacement about the pivot point is equal to the angular displacement at the joint of the magnet due to symmetry. Hence from diagram φ=θ.

$$x_m = 0.065cos\theta + 0.065cos\theta \quad (16)$$

$$x_m = 0.13\ cos\theta \quad (17)$$

$$\dot{x}_m = -0.13\ sin\theta\dot{\theta}\ m \quad (18)$$

The derived equation of motion for the magnet is a function of both the angular displacement and velocity of the cylinder.

4.3 Determination of the Induced EMF

The EMF induced in any conductive coil due to a fluctuating magnetic field is highly dependent on the strength of the magnetic field, the number of coils and the rate of change of flux. The parameters required to determine the magnetic field strength are, the magnetic field strength, conductor area and the height of the windings as shown in Table 1. The conductor wire used for analysis is Grade 12 copper wire. The following assumptions were made to simplify the calculation approach.

Assumptions

Magnetic field lines cut the coils effectively.

They're no hysteresis or eddy current losses within the system.

$$\text{Induced emf, } E = -N \times \frac{d\emptyset_b}{dt} \quad (19)$$

$$\frac{d\emptyset_b}{dt} = \frac{\emptyset_b \times \dot{x}_m}{h} \quad (20)$$

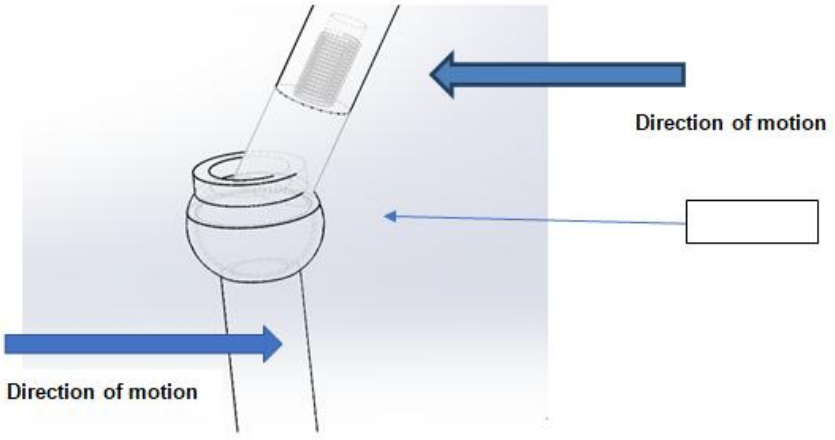

Fig. 8. Joint of the force disc

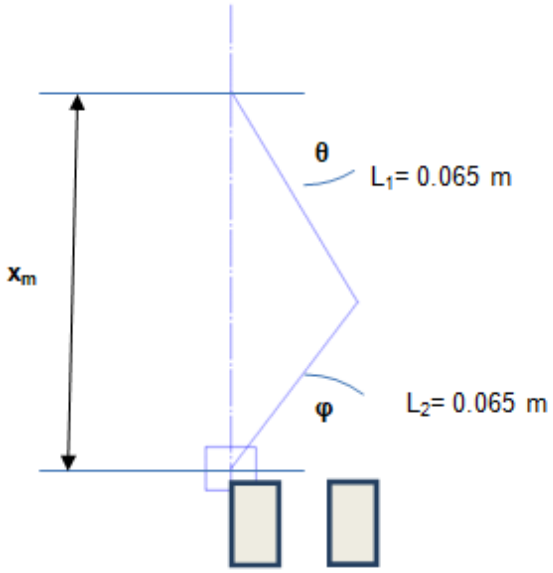

Fig. 9. Joint mechanism of the magnet

Table 1. Generator parameters

Parameter	Value	Units
Magnetic field strength (B)	1.32	T
Mass of magnet	0.0167	kg
Wire radius (r)	2.053×10^{-3}	m
Height of windings (h)	0.15	m
Number of turns	200	

$$\emptyset_b = B \times A \quad (21)$$

$$Wire\ area\ (A) = \pi(2.053 \times 10^{-3})^2$$

$$A = (1.26 \times 10^{-3}) \times 2$$

$$A = 2.52 \times 10^{-3} m^2$$

$$\emptyset_b = 1.32 \times (2.52 \times 10^{-3})$$

$$\emptyset_b = 3.324 \times 10^{-3}\ T.m^2$$

5. RESULTS AND DISCUSSION

5.1 Evaluation of Derived Equations

The solution to the equation of motion was used to plot the behavior of the turbine for a range of wind speeds as shown in Fig. 10. The input parameters into the equation of motion are as shown in Table 2. The angular displacement, angular acceleration and EMF at designed speed of 4m/s, 1m/s and 7m/s are shown in Tables 3,4 and 5 respectively.

Table 2. Equation of motion evaluation parameters

Parameter	Input range	Units
Wind Speed (m/s)	1-13	m/s
Moment (M_o)	0.06762-11.43	N.m
Shedding frequency (ω_s)	10.5-136.14	rad/s
Natural frequency (ω_n)	41.91	rad/s
Equivalent stiffness (k_{eq})	126.82	N/m
Time	0-12	s
Step intervals	0.2	

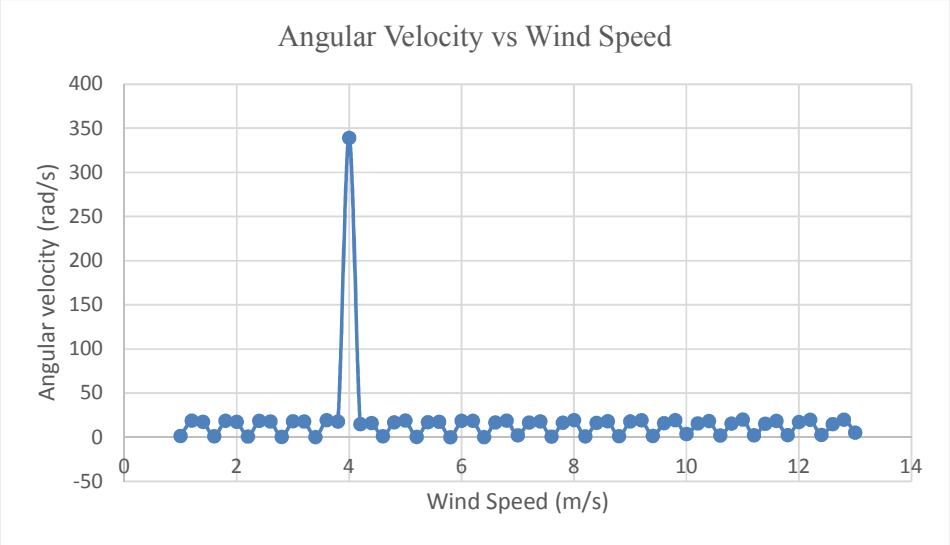

Fig. 10. Comparison of angular velocity and wind speed

Table 3. Calculated results at designed speed of 4m/s

Time (s)	θ (rad)	$\dot{\theta}$ (rad/s)	$\dot{x_m}$ (m/s)	EMF (V)
0.0	0.500	340.470	21.220	94.114
0.2	-0.221	-188.342	5.367	23.804
0.4	-0.277	-151.984	5.409	23.991
0.6	0.500	340.192	21.219	94.112
0.8	-0.227	-188.217	5.505	24.417
1.0	-0.272	-151.831	5.298	23.498
1.2	0.501	339.913	21.215	94.094
1.4	-0.233	-188.089	5.642	25.024
1.6	-0.266	-151.682	5.186	23.002
1.8	0.501	339.635	21.208	94.060
2.0	-0.239	-187.958	5.778	25.625
2.2	-0.260	-151.536	5.074	22.503
2.4	0.501	339.357	21.197	94.012
2.6	-0.245	-187.824	5.912	26.219
2.8	-0.255	-151.392	4.960	22.001
3.0	0.501	339.078	21.182	94.114
3.2	-0.250	-187.687	6.044	23.804
3.4	-0.249	-151.252	4.846	23.991

The response of wind speeds above and below resonance is shown in Fig. 11.

5.2 Power Coefficient Analysis

The efficiency of any wind turbine is determined by the ratio of power extracted from the wind to power available in the wind. The theoretical efficiency will be calculated for the designed wind speed of 4 m/s.

$$C_p = \frac{Power\ Extracted}{Power\ available} \quad (22)$$

$$C_p = \frac{Kinect\ energy\ of\ magnet\ /unit\ time}{Power\ available\ in\ the\ wind} \quad (23)$$

$$Power\ available\ in\ the\ wind = 0.5\rho A v^3$$

$$Power\ available\ in\ the\ wind = 0.5 \times 1.225 \times 0.23 \times 4^3$$

$$Power\ available\ in\ the\ wind = 9.016\ W$$

From Table 6 for t=0.2s the speed of the magnet is 5.637 m/s. The mass of the magnet is

m= 0.0167 kg.

$$Kinect\ energy\ of\ magnet\ /unit\ time = {}^{0.5m(\dot{x}_m)^2}/_{t}$$

$$Kinect\ energy\ of\ magnet\ /unit\ time = {}^{0.5 \times 0.0167 \times (5.367)^2}/_{0.2}$$

$$Kinect\ energy\ of\ magnet\ /unit\ time = 1.203\ W$$

$$C_p = \frac{1.203}{9.016}$$

$$C_p = 0.1338$$

From Fig. 12, the power coefficient peaked at approximately 70% at a time of 0.6s and then reduces to approximately 1%. This significant difference in power harnessed is due to the initial conditions of the system before it reaches steady state. We can see that from 0s seconds to approximately 1.2s the system response is a sinusoidal waveform with high fluctuating magnitude.

A theoretical mechanical vibration analysis model of the bladeless wind turbine was done in order to determine its magnitude of oscillation at a wind

Table 4. Calculated results at wind speed of 1 m/s

Time (s)	θ (rad)	$\dot{\theta}$ (rad/s)	$\dot{x_m}$ (m/s)	EMF (V)
0.0	0.500	1.506	0.094	0.416
0.2	-0.221	-18.860	0.536	2.378
0.4	-0.278	17.498	0.624	2.767
0.6	0.500	1.228	0.077	0.340
0.8	-0.226	-18.735	0.547	2.425
1.0	-0.272	17.651	0.617	2.737
1.2	0.501	0.950	0.059	0.263
1.4	-0.232	-18.608	0.557	2.470
1.6	-0.267	17.800	0.610	2.704
1.8	0.501	0.671	0.042	0.186
2.0	-0.238	-18.477	0.567	2.514
2.2	-0.261	17.946	0.602	2.670
2.4	0.501	0.393	0.025	0.109
2.6	-0.244	-18.342	0.576	2.555
2.8	-0.255	18.089	0.594	2.634
3	0.501	0.114	0.007	0.032
3.2	-0.250	-18.205	0.585	2.595
3.4	-0.249	18.229	0.585	0.013

Table 5. Calculated results for wind speed of 7m/s

Time (s)	θ (rad)	$\dot{\theta}$ (rad/s)	$\dot{x_m}$ (m/s)	EMF (V)
0	0.500	0.569	0.036	0.158
0.2	-0.232	-18.391	0.550	2.438
0.4	-0.266	17.966	0.615	2.726
0.6	0.500	0.292	0.018	0.081
0.8	-0.237	-18.267	0.560	2.482
1	-0.260	18.118	0.607	2.693
1.2	0.500	0.013	0.001	0.004
1.4	-0.243	-18.139	0.569	2.525
1.6	-0.255	18.268	0.599	2.658
1.8	0.501	-0.264	0.017	0.073
2	-0.249	-18.008	0.579	2.566
2.2	-0.249	18.414	0.591	2.622
2.4	0.501	-0.543	0.034	0.150
2.6	-0.255	-17.874	0.587	2.605
2.8	-0.243	18.557	0.582	2.583
3	0.501	-0.822	0.051	0.228
3.2	-0.261	-17.737	0.596	2.642
3.4	-0.238	18.697	0.573	2.542

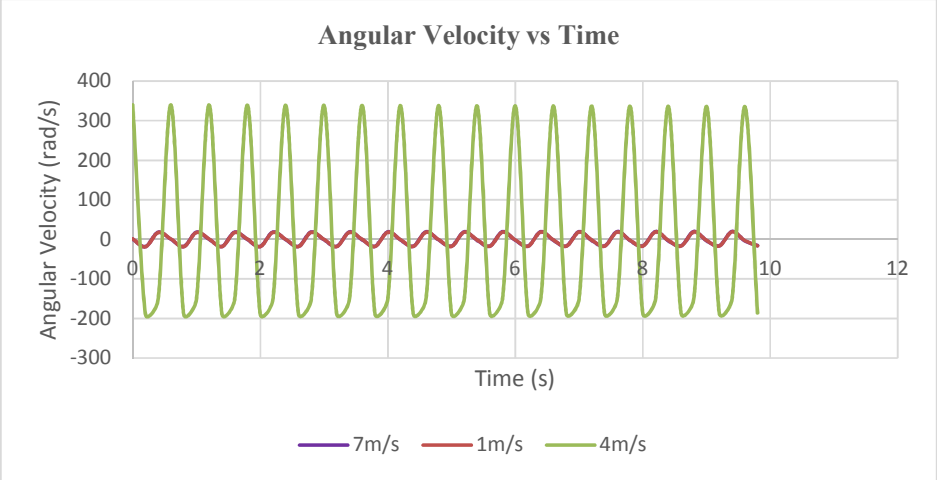

Fig. 11. Response of wind speeds above and below resonance

Table 6.Calculate power and efficiency of the bladeless wind turbine

Time (s)	$\dot{x_m}$ (m/s)	Power (W)	Efficiency (%)
0.0	21.220	0	0
0.2	5.367	1.203	13.338
0.4	5.409	0.611	6.774
0.6	21.219	6.266	69.499
0.8	5.505	0.316	3.508
1.0	5.298	0.234	2.599
1.2	21.215	3.132	34.736
1.4	5.642	0.190	2.105
1.6	5.186	0.140	1.556
1.8	21.208	2.086	23.141
2.0	5.778	0.139	1.545
2.2	5.074	0.098	1.083
2.4	21.197	1.563	17.338
2.6	5.912	0.112	1.244
2.8	4.960	0.073	0.813

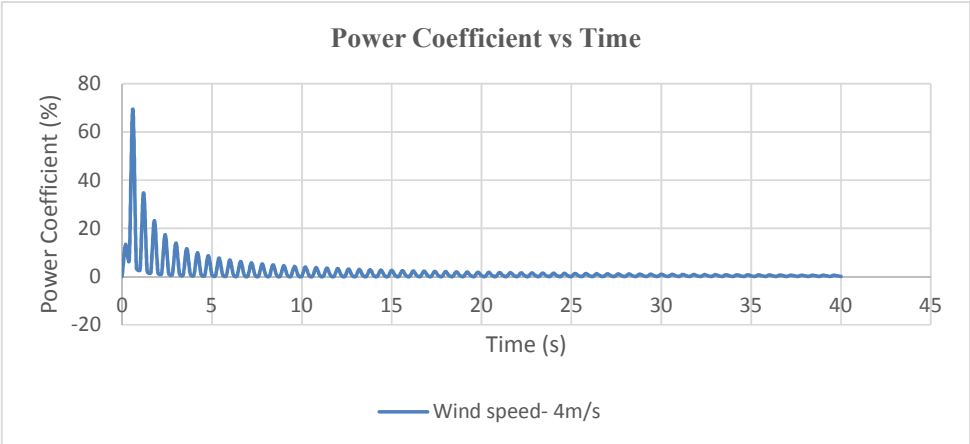

Fig. 12. Power coefficient of bladeless wind turbine

speed of 4 m/s. The proposed model allowed the angle of oscillation about the pivot point to be determine. The angular velocity is determined by the geometrical properties of the cylindrical mast and the wind speed which causes a moment about the pivot point. This is the major performance criteria of the system. For a comprehensive analysis, focus was kept mainly on predicting whether the turbine would behave as expected when compared to the literature, that is, will oscillations only occur at a vortex shedding frequency near to the natural frequency of the system.

It was stated that an oscillating cylinder within a crossflow would oscillate in the transverse direction to the flow. Previous research conducted on flow induced oscillations were done with the main goal of reducing/damping such oscillations during practical applications since resonant conditions can severely damage structures or components. In addition, for what few bladeless wind turbine patents discovered, the designs incorporated the structural support of the cylinder along its center axis. Fixing the support of the structure along its axis is the easiest way to ensure that the system remains standing during operation but as a tradeoff, it limits the oscillation capabilities. This study incorporates structural support at a distance offset from the center axis of the cylindrical mast. Springs were added to the final design as means to provide the stiffness required to obtain resonance with the vortex shedding frequency and to also assist in supporting the structure.

The results obtained showed that for wind speeds above and below the designed wind speed of 4m/s the angular velocity remained the same. Results of this model showed that exactly only at resonance high amplitudes occur. This is expected, but it also shows the weakness of the proposed mathematical model alone to match the findings to that of physical testing and observation. From Fig. 4 It was discovered that for linearly tapered cylinders, increased oscillations occurred during the 'lock-in range' for a range of reduced velocities. The reduced velocity of the proposed final design at 4m/s is approximately Vr = 5. This value lies within the theoretical range lock in range where increased oscillations are expected to occur between reduced velocities of 4.75 and 8 [1]. For this prototype, that correlates to a wind speed of 3.8 m/s to 6.4 m/s. Therefore, in reference to literature, increased oscillations should have occurred during the stated range.

6. CONCLUSION

Utilizing vorticity as a source of generating power is a new concept which is now being recognized. It would be untimely to say that the bladeless wind turbine can prove to be more efficient than the conventional horizontal axis wind turbine (HAWT). However, this technology provides some advantages, for example, with an appropriate design, an oscillating cylinder can harness energy of the wind respective of its direction without significantly limiting the magnitude of the oscillations. This study was carried out with that main point in mind. Results showed that with the current power generating mechanism, the average efficiency attainable is approximately 2% at steady state. This is the theoretical efficiency which could be achieved based on the current model. To reiterate, there is still major room for analysis to obtain the true efficiency of the device as laid out by the literature. With that being said, the results showed that increased effort should be placed in the initial stages of the vibrational analysis to develop a more accurate model to predict the oscillations of the turbine mast.

COMPETING INTERESTS

Authors have declared that no competing interests exist.

REFERENCES

1. Sarpkaya T. Vortex-Induced Oscillations. Journal of Applied Mechanics. 1979;241-258.
2. British Petroleum. Statistical Review of World Energy British Petroleum, London, UK; 2019.
3. Ježov J. Pressure Sensitive Lateral Line for Underwater Robot. Thesis on Informatics and System Engineering C89. TUT Press, Tallinn University of Technology Tallinn, Estonia; 2013.
Available:Https://Www.Researchgate.Net/Figure/Schematic-Of-A-Karman-Vortex-Street-Laminar-Flow-From-The-Left-Is-Obstructed-By-A_Fig2_283776953
4. Kaneko, Shigehiko, Tomomichi Nakamura, Fumio Inada, Minoru Kato, Kunihiko Ishihara, Takashi Nishihara, and Mikael A. Langthjem. Vibration induced by cross-flow. In Flow-Induced Vibrations, by Shigehiko Kaneko, Tomomichi Nakamura, Fumio Inada, Minoru Kato, Kunihiko Ishihara, Takashi Nishihara, Mikael A.

Langthjem. New York: Academic Press. 2014;29-109.

5. Lin, Zhonglu. Numerical Study of the Interaction between Fluid and Multiple Cylinders. First Year Report. 2016;1-79.
6. Lienhard John H. University of Houston Research. University of Houston Web site; 1966. January 1. Accessed October 24, 2019. Available:http://www.uh.edu/engines/vortexcylinders.pdf.
7. Barrero-Gil, Antonio. Extracting energy from Vortex Induced Vibrations: A parametric study. Applied Mathematical Modelling. 2012;3153-3160.
8. Óskarsdóttir, Margrét Ósk. A General Description and Comparison of Horizontal Axis Wind Turbines and Vertical Axis Wind Turbines; 2014.
9. Hassan RED, Bishop AY. The lift and drag forces on a circular cylinder in a flowing fliud. Fluid Induced Vibrations. 1963;32-50.
10. Seyed-Aghazadeh, Banafsheh, and Daniel W, Modarres-Sadeghi, Yahya Carlson. The influence of taper ratio on vortex-induced vibration of tapered cylinders in the crossflow direction . Journal of Fluids and Structures; 2014.
11. Vinod R. Challa, Prasad MG, Yong Shi, Frank T. Fisher. A vibration energy harvesting device with bidirectional resonance frequency tunability. Smart Materials and Structures. 2008;1-11.

Peer-review history:
The peer review history for this paper can be accessed here:
http://www.sdiarticle4.com/review-history/63908